

Measurements of Hydroxyl and Hydroperoxy Radicals during CalNex-LA:

Model Comparisons and Radical Budgets

S. M. Griffith^{1,2}, R. F. Hansen^{3,4}, S. Dusanter^{1,5}, V. Michoud^{7,8}, J. B. Gilman^{9,10}, W. C. Kuster⁹, P. R. Veres^{9,10}, M. Graus^{9,10,11}, J. A. de Gouw⁹, J. Roberts^{9,10}, C. Young^{9,10,12}, R. Washenfelder^{9,10}, S. S. Brown^{9,10}, R. Thalman¹³, E. Waxman¹³, R. Volkamer¹³, C. Tsai¹⁴, J. Stutz¹⁴, J. H. Flynn¹⁵, N. Grossberg¹⁵, B. Lefer^{15,16}, S. L. Alvarez¹⁵, B. Rappenglueck¹⁵, L. H. Mielke^{17,18}, H. D. Osthoff¹⁷, and P. S. Stevens^{1,3}

¹School of Public and Environmental Affairs, Indiana University, Bloomington, Indiana, USA, ²Now at Department of Chemistry, The Hong Kong University of Science and Technology, Hong Kong, China, ³Department of Chemistry, Indiana University, Bloomington, Indiana, USA, ⁴ Now at School of Chemistry, University of Leeds, Leeds, UK, ⁵Mines Douai, SAGE, F-59508 Douai, France, ⁶Université de Lille, Lille, France, ⁷LISA/IPSL, Laboratoire Interuniversitaire des Systèmes Atmosphériques, UMR CNRS 7583, Université Paris Est Créteil(UPEC) et Université Paris Diderot (UPD), Créteil, France, ⁸Now at Mines Douai, SAGE, F-59508 Douai, France, ⁹Cooperative Institute for Research in Environmental Sciences, University of Colorado, Boulder, CO, USA, ¹⁰Chemical Sciences Division, Earth System Research Laboratory, National Oceanic and Aeronautic Administration, Boulder, Colorado, USA, ¹¹Now at Institute of Atmospheric and Cryospheric Sciences, Innsbruck University, Austria, ¹²Now at Department of Chemistry, Memorial University of Newfoundland, St. John's, Newfoundland and Labrador, Canada, ¹³Department of Chemistry and Biochemistry and CIRES, University of Colorado at Boulder, Boulder, CO, USA, ¹⁴Department of Atmospheric and Oceanic Sciences, University of California Los Angeles, Los Angeles, California, USA, ¹⁵Department of Earth and Atmospheric Sciences, University of Houston, Texas, USA, ¹⁶Now at Earth Science Division, NASA Headquarters, Washington, DC, USA, ¹⁷Department of Chemistry, University of Calgary, Calgary, Alberta, Canada, ¹⁸Now at Department of Chemistry, University of Indianapolis, Indianapolis, Indiana, USA

Contents of this file

Text S1 to S11
Figures S1 to S9
Table S1

Introduction

This supporting material provides more detailed information about the HO_x measurements, including the ozone-water interference and the correlation of the OH measurements with J(O1D). Additional information about the supporting measurements that were used to constrain the box model as well as how the modeled HO₂* was derived and how it was constrained to the measured reactivity are also included. Additional details are provided concerning comparisons with previous measurements, the radical budgets, the HONO production and loss imbalance, the NO_x dependence of the HO_x measured and model agreement, and the treatment of PANs in the model.

S1: Notes on Supporting Measurements

For the CalNex-LA modeling, a few key constraints did not have complete measurement coverage throughout the whole campaign. NO₂ measured by the University of Houston group and co-located with the IU-FAGE instrument began in the morning of May 27th. Before that time, NO₂ measured by the NOAA IBBCEAS instrument, which was also co-located with the IU-FAGE instrument was used. Correlations of the NOAA and the University of Houston NO₂ data after May 27th were very good ($R^2 > 0.95$) and agreed to within $\pm 10\%$. For periods where there were long simultaneous gaps in these two measurements, NO₂ measurements from the University of Colorado CE-DOAS instrument a few kilometers away (at 37 m altitude) was used to constrain the model. Correlations between University of Colorado and University of Houston NO₂ concentrations after May 27th were good ($R^2 > 0.85$) and corrections of 0.72 and 0.87 were applied to the daytime and nighttime respectively to account for systematic differences in the data. Measurements of HONO by the NOAA IBBCEAS instrument and co-located with the IU-FAGE instrument began on the evening of May 26th, but two other HONO measurements were available throughout the campaign. Both alternate measurements of HONO were performed at different heights and by different techniques. For the times preceding the evening of May 26th, the NOAA/Univ. of Colorado CIMS HONO measurement was used, which was located a few meters below the IU-FAGE instrument, and a correction of 0.83 ($R^2 = 0.78$) was applied to account for differences in height between the

IBBCEAS and CIMS instruments and the vertical distribution of HONO. Finally, glyoxal measurements also performed by NOAA with the IBBCEAS instrument did not begin until the evening of May 26th. For measurements prior to this date, measurements of glyoxal from the University of Colorado CE-DOAS instrument were used ($R^2 = 0.46$) with a daytime correction of 0.76, and using the nighttime average from May 26th – June 16th. Methane and hydrogen mixing ratios were fixed at 2.0 ppmv and 500 ppbv respectively [Peischl, *et al.*, 2013].

S2: Ozone × Water × Power Interference during CalNex

To account for the photolytic ozone-water interference and any other potential interferences detected by IU-FAGE, a titration system for external C_3F_6 addition above the sampling nozzle was installed. The external C_3F_6 addition was used throughout the campaign, introduced sequentially with spectral modulation OH measurements in a duty cycle of 40 cycles (tuning on and off the OH transition) of spectral modulation OH followed by 20 cycles of C_3F_6 addition (Figure S1, top), and the signal from C_3F_6 addition cycles were subtracted from the signal from the spectral modulation cycles. The measured interference was consistent with that expected from the laser photolysis of ambient mixing ratios of O_3 and subsequent reaction with water vapor (reactions R1 and R2). Based on laboratory calibrations of the interference as a function of ozone, water vapor, and laser power, the calculated interference was within their combined uncertainties (Figure S1, bottom).



S3: Model Derived Carbonyls

To gain insights into the measurement-model discrepancies, the base RACM2 model was modified to constrain the model derived dicarbonyl concentrations, which as a radical source could impact the modeled HO_x concentrations. Gas-phase dicarbonyls are known to be significantly affected by physical

loss processes [Edwards *et al.*, 2013], thus these and other long-lived compounds that are unconstrained in the model may require an added non-chemical loss (i.e. dilution) to accurately reflect their ambient concentrations [Dusanter *et al.*, 2009b; Volkamer *et al.*, 2010]. To account for additional losses, the RACM2 derived concentrations of methylglyoxal (MGLY) and dicarbonyls (DCB) were constrained by the same factor required to bring the modeled glyoxal concentrations into agreement with the measurements (approximately a factor of 2-3 during the day). This is a reasonable method to constrain MGLY and DCB since glyoxal also has similar sources and sinks. However, constraining MGLY and DCB using this method only reduced OH concentrations by less than 5% and HO₂* by less than 10%, which could not explain the observed discrepancy between the base RACM2 modeled OH and that observed during the weekends + holiday.

S4: Model derived HO₂*

All of the RACM2 peroxy radical categories used in determining the modeled HO₂* concentrations from Eq. 1 with their corresponding conversion efficiencies under the operating conditions of IU-FAGE during CalNex-LA are listed in Table 3. A detection efficiency of 1.0 ± 0.5 was used for peroxy radicals derived from terminal and internal olefins (OLTP and OLIP), monoterpenes (APIP, LIMP), and unsaturated aldehydes (UALP). A detection efficiency 0.80 ± 0.14 was used for peroxy radicals derived from isoprene (ISOP), toluene (TLP1, TOLP, TR2, PER1, PER2) benzaldehyde and other aromatic aldehydes (BALP, BAL1, BAL2), benzene (BENP), ethene (ETEP), methacrolein (MACP, MCP), methylvinyl ketone (MVP), and xylenes (XY2, XYL1, XYLP, XYO2, XYOP). A detection efficiency of 0.6 ± 0.3 was used for peroxy radicals derived from C8-C10 alkanes (HC8P). A detection efficiency of 0.3 ± 0.15 was used for peroxy radicals from C5-C7 alkanes (HC5P). A detection efficiency of 0.15 ± 0.04 was used for peroxy radicals derived alkanes, esters and alkynes (HC3P) and higher saturated acyl peroxy radicals (RCO3). A detection efficiency of 0.07 ± 0.03 was estimated for peroxy radicals derived from methane (CH3O2), ethane (ETHP), acetone (ACTP), ketones (KETP, methyl ethyl ketone (MEKP), acyl peroxy radicals (ACO3), and acetic and higher acids (ORAP).

S5: Correlation of OH with J(O¹D)

During CalNex-LA, J(O¹D) photolysis rates were observed to correlate well with measured OH concentrations ($R^2 = 0.74$) (Figure S2) but explained less of the variability than the J(O¹D) vs. OH relationships reported in Rohrer and Berresheim [2006] ($R^2 = 0.85-0.95$). The correlation between the weekends and weekdays were not significantly different ($R^2 = 0.72, 0.75$ for weekend and weekday) and introducing the product of J(O¹D) \times [O₃], J(O¹D) \times [H₂O] or J(O¹D) \times [O₃] \times [H₂O] did not improve the correlation. The J(O¹D) vs. OH data was also fitted to an empirical power-law function (Eq.1) as in Rohrer and Berresheim [2006], where [OH] is in units of molecules cm⁻³ / 10⁶ and JO¹D photolysis rates are in units of s⁻¹ / 10⁻⁵:

$$[OH] = a(J(O^1D))^b + c \quad \text{Eq. S1}$$

Comparing the results of the power-law dependence of [OH] on J(O¹D) from the CalNex-LA site to those detailed in Rohrer and Berresheim [2006], we find that the CalNex-LA results ($a=1.7, b=0.88, c$ below the limit of detection) were similar to that for the BERLIOZ campaign (Holland et al., 2003) for NO_x and CO mixing ratios and total OH reactivity [Konrad et al., 2003] similar to that observed during CalNex-LA (Figure S3). The pre-exponential component (a) was slightly greater for the BERLIOZ J(O¹D) vs. OH relationship (CalNex-LA = 1.7; BERLIOZ = 2) suggesting that OH chemistry during BERLIOZ had a stronger relative dependence on reactants such as NO_x and VOCs than on photolytic processes.

S6: Comparison to other urban HO_x measurements

The average peak concentrations of OH and HO₂* measured during CalNex-LA were similar to that observed in other urban areas (Table 1). Average peak OH concentrations in these studies ranged from 2.2×10^6 cm⁻³ measured during the TORCH campaign in Essex, UK [Emmerson et al., 2007] to approximately 13×10^6 cm⁻³ measured during the PRIDE campaign in the Pearl River Delta, China that

measured total OH radical reactivity up to $\sim 20 \text{ s}^{-1}$ [Hofzumahaus *et al.*, 2009; Lu *et al.*, 2012], which can be compared to the peak measured OH and OH radical reactivity values of approximately $4 \times 10^6 \text{ cm}^{-3}$ and 20 s^{-1} observed during CalNex-LA. The high concentrations of OH measured during the PRIDE campaign could not be explained by models, suggesting that a significant source of OH radicals was missing from the model [Lu *et al.*, 2012], in contrast to the results reported here for CalNex-LA. Although the noontime OH reactivity during the PRIDE campaign was similar to that measured during CalNex-LA, mixing ratios of NO were lower (0.1-0.2 ppbv) and mixing ratios of isoprene were higher (typically 1-2 ppbv). Under these high isoprene/low NO conditions, Lu *et al.* [2012] found that including several proposed OH radical recycling mechanisms, including the isomerization of isoprene peroxy radicals [Peeters *et al.*, 2009; Peeters and Müller, 2010] improved the measurement/model agreement, although recent laboratory studies and updates to the mechanism suggest that the efficiency of OH radical cycling by this mechanism may be less than originally proposed [Crouse *et al.*, 2011; Lu *et al.*, 2012; Peeters *et al.*, 2014]. Although these OH-radical recycling mechanisms were not included in the analysis presented here, it is likely that these reactions cannot compete with the rate of the competing $\text{RO}_2 + \text{NO}$ reaction under the high mixing ratios of NO observed during CalNex-LA [Peeters and Müller, 2010].

Average peak reported HO_2 concentrations ranged from $1.5 \times 10^8 \text{ cm}^{-3}$ measured during the PMTACS campaign in New York City [Ren *et al.*, 2003a] and the IMPACT campaign in Tokyo [Kanaya *et al.*, 2007] to $1.5 \times 10^9 \text{ cm}^{-3}$ observed during the CARE campaign in Beijing [Lu *et al.*, 2013], similar to the measured HO_2^* concentrations $2\text{-}5 \times 10^8 \text{ cm}^{-3}$ observed during CalNex-LA. Mao *et al.* [2010] demonstrated through an analysis of photochemical activity at multiple field campaigns that in general HO_2 anti-correlates with the ratio of NO_x to non-methane VOCs (NO_x/NMVOC in ppbv/ppbC) as HO_2 concentrations tend to decrease with increasing NO (increased titration) and NO_2 (greater OH loss) while greater NMVOC levels tend to increase HO_2 concentrations through oxidation by OH. For example, the NYC2001 campaign during PMTACS exhibited the highest NO_x/NMVOC levels (approximately 0.2 at midday) and relatively low HO_2 concentrations (approximately $1.5 \times 10^8 \text{ cm}^{-3}$), while the TRAMP2006 campaign exhibited relatively low midday NO_x/NMVOC levels (approximately 0.02) and relatively high

HO₂ concentrations (approximately $12 \times 10^8 \text{ cm}^{-3}$) compared to other urban field campaigns.

Weekday HO₂* concentrations observed during CalNex-LA were similar to reported HO₂ concentrations observed during the NYC2001 campaign [Ren *et al.*, 2003a,b]. Measured mixing ratios of VOCs and NO_x during CalNex-LA resulted in a NO_x/NMVOC ratio of approximately 0.15 (Figure S4) similar to that found for the NYC2001 campaign, although NO_x levels were systematically higher for New York City. However, measured total OH reactivity during CalNex was similar to that observed during NYC2001, suggesting that the effective NO_x/NMVOC ratio during CalNex-LA was lower than NYC2001 given the significant missing reactivity observed during CalNex-LA that was not observed during NYC2001 [Ren *et al.*, 2003b], although the NMVOC concentration may not scale with the OH reactivity. Peak OH concentrations observed during NYC2001 were about a factor of two greater on average than the weekday CalNex-LA OH concentrations reported here, which may reflect the higher NO_x levels observed during NYC2001.

Weekend HO₂* concentrations at CalNex-LA were greater than the HO₂ concentrations reported during NYC2001 but were similar to the reported HO₂ measurements made during TEXAQS2000, consistent with the low NO_x/NMVOC ratio observed at these sites [Mao *et al.*, 2010]. However, measured OH concentrations during TEXAQS2000 were a factor of two greater on average than CalNex-LA. The observed OH reactivity during weekends at CalNex-LA were approximately two times greater than TEXAQS2000, suggesting that the effective NO_x/NMVOC ratio during the weekends at CalNex-LA was lower given the agreement between measured and calculated reactivity during TEXAQS2000 [Mao *et al.*, 2010]. The higher OH reactivity could in part explain the lower observed OH concentrations at CalNex-LA under the relatively low- NO_x conditions observed at these sites [Mao *et al.*, 2010].

The measured HO₂*/OH ratio during CalNex-LA was a factor of 4-5 times greater than the HO₂/OH ratio measured during the NYC2001 campaign for the same NO mixing ratio [Ren *et al.*, 2003a], suggesting that the RO_x cycling may differ between the campaigns. Although the measured total OH reactivity was similar, the measured reactivity during NYC2001 was consistent with the calculated reactivity in contrast to the significant missing reactivity measured during CalNex-LA. The missing reactivity at

CalNex-LA may contribute to the difference in radical cycling at these two sites. In contrast, the HO₂/OH ratios observed in Mexico City during the MCMA-2003 [Shirley *et al.*, 2003; Sheehy *et al.*, 2010] and MCMA-2006 [Dusanter *et al.*, 2009a,b] campaigns were similar to the HO₂*/OH ratios observed during CalNex-LA, suggesting that HO_x radical cycling were similar. The observed concentrations of OH and HO₂ were somewhat higher during MCMA-2003 compared to the OH and HO₂* measurements during CalNex-LA although the measured noontime reactivity was similar [Shirley *et al.*, 2006], while the measured concentrations of OH and HO₂ during MCMA-2006 were similar to the CalNex-LA measurements for a similar calculated total OH reactivity [Dusanter *et al.*, 2009] (Table 1). Although the mixing ratios of ozone, NO_x, VOCs, and the rates of radical initiation during the MCMA campaigns were higher than observed during CalNex-LA [Dusanter *et al.*, 2009b; Volkamer *et al.*, 2010], the NO_x/NMVOC ratios would be similar after accounting for the missing reactivity observed during CalNex-LA. An analysis of potential sources of the missing OH reactivity will be discussed in a future publication [Hansen *et al.*, in preparation].

S7: Modeling the missing reactivity

The reactivity from the lumped species in the RACM2 base model can be calculated from:

$$k_{OH}^L = \sum_i^N k_{OH+x_i}^{II} [x_i]_{meas} \quad \text{Eq. S2}$$

Here k_{OH}^L is the OH reactivity calculated from the constrained lumped species used by the base model which is a portion of the total OH reactivity, k_{OH} . The missing reactivity is determined from the difference between the calculated reactivity from constrained lumped species and the measured total reactivity:

$$k_{OH}^{miss} = k_{OH}^{meas} - k_{OH}^L \quad \text{Eq. S3}$$

Using these reactivity values, a multiplier can be calculated by which to enhance the selected lumped species in the model:

$$\beta_{OHr} = \frac{k_{OH}^L + k_{OH}^{miss}}{k_{OH}^L} \quad \text{Eq. S4}$$

$$[x_i]_{mOHr} = \beta_{OHr} \times [x_i]_{meas} \quad \text{Eq. S5}$$

β_{OHr} is the multiplicative factor used to calculate the VOC concentration of each constrained lumped species, $[x_i]_{mOHr}$, to match the measured reactivity in the increased reactivity scenario. The new OH reactivity contribution from all the constrained lumped species, $k_{OH}^{L,mOHr}$, can then be calculated by:

$$k_{OH}^{L,mOHr} = \sum_i^N k_{OH+x_i}^{II} [x_i]_{mOHr} \quad \text{Eq. S6}$$

Several sets of VOCs were tested to increase the total OH reactivity, but only two are described here:

1) Mixed VOC set #1 assumes that the missing reactivity consists of a mix of saturated VOCs and aldehydes similar to that observed by increasing the reactivity of the constrained saturated VOCs and aldehydes in the model (HC3, HC5, HC8, ALD). Reactive unsaturated species are not included in the missing reactivity.

2) Mixed VOC set #2 assumes that the missing reactivity consists primarily of oxygenated species by increasing the reactivity of aldehydes and alcohols in the model (ALD, ROH). Saturated and unsaturated VOCs are not included in the missing reactivity.

Figure S5 demonstrates the impact of the different missing reactivity VOC set used to enhance OH reactivity in the model. As illustrated in this Figure, changing the missing reactivity from a mix of saturated and oxygenated species (blue line) to a mix of oxygenated species (red line) has a negligible impact on the weekday OH and HO₂* concentrations. However, assuming the missing reactivity is a mix of oxygenated species (VOC mix #2) does increase the modeled weekend concentration of OH and to a lesser extent HO₂*, while the agreement with the measured OH concentrations on the weekend is better with VOC mix #1. Including unsaturated VOCs in the missing reactivity scenario significantly increases the nighttime HO₂* concentrations due to the increased radical production from ozonolysis (not shown). Overall, this suggests that the ‘missing’ reactivity at the CalNex-LA site primarily consists of saturated hydrocarbons, aldehydes, and less reactive aromatics.

S8: NO_x dependence of the HO_x measured and model agreement

Figure S6 shows correlation plots for the model vs. measurements as a function of mixing ratios of NO_x for both OH and HO₂*. Under the higher NO_x conditions observed during the week, the modeled OH is in good agreement with the measured OH. The discrepancy between the model and the measurements is greatest on the lower NO_x conditions observed on the weekends when NO_x is less than 5 ppb. In contrast, the greatest underestimation of HO₂* by the model occurs on the higher NO_x conditions observed during the week when NO_x mixing ratios are greater than 15 ppb, while the model is in good agreement with the measurements during the lower NO_x conditions observed on the weekends.

S9: PANs in the Model

Konrad et al. [2003] demonstrated the importance of constraining PAN concentrations in order to properly simulate peroxy radical concentrations in an urban area. For the CalNex-LA site, unconstraining PAN concentrations results in modeled OH concentrations that were 15% greater than the constrained base RACM2 model. Figure S7 (top plot) illustrates that the base model tends to underestimate the measured diurnal average daytime PAN concentration. However, the increased OH reactivity scenario better simulates the measured PAN concentrations, suggesting that properly representing the OH reactivity may be important in order to properly simulate other important compounds such as the PAN NO_x reservoirs. Figure S7 (bottom) also illustrates the ability of the RACM mechanisms to balance PAN production and loss in their respective chemical mechanisms. The PAN equilibrium chemistry is improved in the RACM2 mechanism compared to the original RACM mechanism including the Mainz Isoprene Mechanism (RACM-MIM) as indicated by the balance of production ($\text{RO}_2 + \text{NO}_2 \rightarrow \text{PANs}$) and loss ($\text{PANs} \rightarrow \text{RO}_2 + \text{NO}_2$).

S10: OH, HO₂, and RO₂ Radical Budgets

Table S1 displays the percent contribution of RO_x radical initiation routes across non-winter ur-

ban campaigns. This table illustrates the differences in reporting these various contributions for the different campaigns. Often the net contribution of HONO photolysis as a radical source is reported as opposed to the gross contribution reported here. Discussion of these percent contributions is given in the main text.

Figure S8 shows the average diurnal OH, HO₂, and RO₂ radical budgets for the weekends + holiday (left) and weekdays (right) including radical initiation, termination and propagation. As illustrated in this Figure, rates of radical propagation are significantly greater than rates of radical initiation and termination during CalNex-LA and the rates of radical production and loss is balanced for each radical. Percent contributions of the propagation routes to total production and loss for each RO_x radical indicate that OH initiation and termination is balanced in this urban environment, while the rate of HO₂ radical initiation from formaldehyde and carbonyls is greater than termination and the rate of RO₂ radical termination through organic nitrate formation is greater than initiation. Total radical initiation and termination is balanced (Figure 8 in the main text).

S11: HONO production and loss imbalance

As mentioned in the main text, nitrous acid (HONO) is a primary contributor to new radical formation on the weekends and weekdays at the CalNex-LA site. Figure S9 shows the imbalance in the rates of HONO production from the gas phase OH + NO reaction and loss from photolysis in the model suggesting the existence of an additional HONO source, similar to that observed in other areas [*Alicke et al.*, 2003; *Czader et al.*, 2012; *Wong et al.*, 2012; *Li et al.*, 2010]. For the weekday average, the magnitude of this additional source(s) is approximately 750 pptv hr⁻¹ at midday and greater than 1 ppbv/hr during the weekends + holiday. The existence of a strong vertical gradient of HONO at the CalNex-LA site suggest a significant source of HONO at the surface [*Young et al.*, 2012], similar to that observed at other urban sites [*Czader et al.*, 2012; *Wong et al.*, 2011]. The additional HONO source correlates well with the product of J(NO₂) * NO₂ and shows a steeper dependence for the lower NO_x weekends at CalNex-LA. However, Lee et al. [2013] recently demonstrated that in an urban area, poor mixing of NO from local

exhaust emissions can enhance gas phase HONO production from the OH + NO reaction leading to an apparent imbalance relative to the rate of HONO photolysis. Uncertainties associated with the photolysis rate of HONO may also impact the imbalance [Volkamer *et al.*, 2010].

S11: The analytical expression for LN/Q

Equations S7-S10 describe the analytical expression for LN/Q as developed by, Kleinman *et al.* [2001]. For the calculation of α , measurements of total OH reactivity were used for the quantity $k_{OH+VOC}[VOC]$, and the calculation of Q used the measurements described in the main text:

$$L_N/Q = -\alpha/2 + \frac{(\alpha^2+4\alpha)^{1/2}}{2} \quad \text{Eq. S7}$$

$$\alpha = \left(\frac{k_{OH+NO_2}[NO_2]k_{HO_2+NO}[NO]\gamma}{k_{OH+VOC}[VOC]} \right)^2 \left(\frac{1}{2Qk_{eff}} \right) \quad \text{Eq. S8}$$

$$\gamma = \frac{[HO_2]}{[HO_2+RO_2]} \quad \text{Eq. S9}$$

$$k_{eff} = k_{HO_2+HO_2}(\gamma^2) + k_{RO_2+HO_2}(\gamma - \gamma^2) \quad \text{Eq. S10}$$

References

- Alicke, B., Platt, U., and Stutz, J. (2002), Impact of nitrous acid photolysis on the total hydroxyl radical budget during the Limitation of Oxidant Production/Pianura Padana Produzione di Ozono study in Milan, *Journal of Geophysical Research-Atmospheres*, 107, 8196, 10.1029/2000JD000075.
- Alicke, B., Geyer, A., Hofzumahaus, A., Holland, F., Konrad, S., Patz, H. W., Schafer, J., Stutz, J., Volz-Thomas, A., and Platt, U. (2003), OH formation by HONO photolysis during the BERLIOZ experiment, *J. Geophys. Res.*, 108, 10.1029/2001jd000579.
- Crounse, J. D., Paulot, F., Kjaergaard, H. G., and Wennberg, P. O. (2011), Peroxy radical isomerization in the oxidation of isoprene, *Phys. Chem. Chem. Phys.*, 13, 13607–13613, doi:10.1039/c1cp21330j, 2011.
- Czader, B. H., Rappenglück, B., Percell, P., Byun, D. W., Ngan, F., and Kim, S. (2012), Modeling nitrous acid and its impact on ozone and hydroxyl radical during the TEXAS Air Quality Study 2006, *Atmos. Chem. Phys.*, 12, 6939-6951, 2012
- Dusanter, S., Vimal, D., Stevens, P. S., Volkamer, R., and Molina, L. T., (2009a), Measurements of OH and HO₂ concentrations during the MCMA-2006 field campaign - Part 1: Deployment of the Indiana University laser-induced fluorescence instrument, *Atmos. Chem. Phys.*, 9, 1665-1685.
- Dusanter, S., Vimal, D., Stevens, P. S., Volkamer, R., Molina, L. T., Baker, A., Meinardi, S., Blake, D., Sheehy, P., Merten, A., Zhang, R., Zheng, J., Fortner, E. C., Junkermann, W., Dubey, M., Rahn, T., Eichinger, B., Lewandowski, P., Prueger, J., and Holder, H. (2009b), Measurements of OH and HO₂ concentrations during the MCMA-2006 field campaign - Part 2: Model comparison and radical budget, *Atmos. Chem. Phys.*, 9, 6655-6675.
- Edwards, P. M., C. J. Young, K. C. Aikin, J. A. de Gouw, W. P. Dubé, F. Geiger, J. Gilman, D. Helmig, J. S. Holloway, J. Kercher, B. Lerner, R. Martin, R. McLaren, D. D. Parrish, J. Peischl, J. M. Roberts, T. B. Ryerson, J. A. Thornton, C. Warneke, E. J. Williams, and S. S. Brown (2013), Ozone photochemistry in an oil and natural gas extraction region during winter: Simulations of a snow-free season in the Uintah Basin, Utah, *Atmos. Chem. Phys.*, 13, 8955-8971, doi:10.5194/acp-13-8955-2013.
- Emmerson, K. M., Carslaw, N., Carpenter, L. J., Heard, D. E., Lee, J. D., and Pilling, M. J. (2005), Urban atmospheric chemistry during the PUMA campaign 1: Comparison of modelled OH and HO₂ concentrations with measurements, *J. Atmos. Chem.*, 52, 143-164, 10.1007/s10874-005-1322-3.
- Emmerson, K. M., Carslaw, N., Carslaw, D. C., Lee, J. D., McFiggans, G., Bloss, W. J., Gravestock, T., Heard, D. E., Hopkins, J., Ingham, T., Pilling, M. J., Smith, S. C., Jacob, M., and Monks, P. S. (2007), Free radical modelling studies during the UK TORCH Campaign in Summer 2003, *Atmos. Chem. Phys.*, 7, 167-181.
- Gear, C. W., *Numerical Initial Value Problems in Ordinary Differential Equations*, Prentice-Hall, Englewood Cliffs, N.J., 1971.

- George, L. A., Hard, T. M., and O'Brien, R. J. (1999), Measurement of free radicals OH and HO₂ in Los Angeles smog, *J. Geophys. Res.*, 104, 11643-11655.
- Griffin, R. J., Dabdub, D., Seinfeld, J. H. (2002), Secondary organic aerosol 1. Atmospheric chemical mechanism for production of molecular constituents, *Journal of Geophysical Research-Atmospheres*, 107, D17, 4332, doi:10.1029/2001JD000541.
- Griffin, R. J., Revelle, M. K., Dabdub, D. (2004a), Modeling the Oxidative Capacity of the Atmosphere of the South Coast Air Basin of California. 1. Ozone Formation Metrics, *Environmental Science and Technology*, 38, 746-752.
- Griffin, R. J. (2004b), Modeling the Oxidative Capacity of the Atmosphere of the South Coast Air Basin of California. 2. HO_x Radical Production, *Environmental Science and Technology*, 38, 753-757.
- Kanaya, Y., Cao, R. Q., Akimoto, H., Fukuda, M., Komazaki, Y., Yokouchi, Y., Koike, M., Tanimoto, H., Takegawa, N., and Kondo, Y. (2007), Urban photochemistry in central Tokyo: 1. Observed and modeled OH and HO₂ radical concentrations during the winter and summer of 2004, *J. Geophys. Res.*, 112, 10.1029/2007jd008670.
- Kleinman, L. I., Daum, P. H., Lee, Y. N., Nunnermacker, L. J., Springston, S. R., Weinstein-Lloyd, J., and Rudolph, J. (2001), Sensitivity of ozone production rate to ozone precursors, *Geophys. Res. Lett.*, 28, 2903-2906, 10.1029/2000gl012597, 2001.
- Konrad, S., Schmitz, Th., Buers, H.-J., Houben, N., Mannschreck, K., Mihelcic, D., Müsgen, P., Pätz, H.-W., Holland, F., Hofzumahaus, A., Schäfer, H.-J., Schröder, S., and Volz-Thomas, A. (2003), Hydrocarbon measurements at Pabstthum during the BERLIOZ campaign and modeling of free radicals, *J. Geophys. Res.*, 108, D4, 8251, 10.1029/2001JD000866.
- Li, G., Lei, W., Zavala, M., Volkamer, R., Dusanter, S., Stevens, P., and Molina, L. T. (2010), Impacts of HONO sources on the photochemistry in Mexico City during the MCMA-2006/MILAGO Campaign, *Atmos. Chem. Phys.*, 10, 6551-6567, 10.5194/acp-10-6551-2010.
- Peeters, J.; Nguyen, T. L.; Vereecken, L. (2009), HO_x radical regeneration in the oxidation of isoprene. *Phys. Chem. Chem. Phys.*, 11, 5935–5939.
- Peeters, J. and Müller, J.-F. (2010), HO_x radical regeneration in isoprene oxidation via peroxy radical isomerisations. II: experimental evidence and global impact, *Phys. Chem. Chem. Phys.*, 12, 14227–14235, doi:10.1039/c0cp00811g.
- Peeters, J., J.-F. Müller, T. Stavrou, and V. S. Nguyen (2014), Hydroxyl Radical Recycling in Isoprene Oxidation Driven by Hydrogen Bonding and Hydrogen Tunneling: The Upgraded LIM1 Mechanism, *J. Phys. Chem. A*, 118(38), 8625-8643.
- Lu, K. D., Rohrer, F., Holland, F., Fuchs, H., Bohn, B., Brauers, T., Chang, C. C., Häsel, R., Hu, M., Kita, K., Kondo, Y., Li, X., Lou, S. R., Nehr, S., Shao, M., Zeng, L. M., Wahner, A., Zhang, Y. H., and Hofzumahaus, A. (2012), Observation and modeling of OH and HO₂ concentrations in the Pearl River Delta 2006: a missing OH source in a VOC rich atmosphere, *Atmos. Chem. Phys.*, 13, 1541-1569.
- Lu, K. D., Hofzumahaus, A., Holland, F., Bohn, B., Brauers, T., Fuchs, H., Hu, M., Häsel, R., Kita, K., Kondo, Y., Li, X., Lou, S. R., Oebel, A., Shao, M., Zeng, L. M., Wahner, A., Zhu, T., Zhang, Y. H., and

Rohrer, F. (2013), Missing OH source in a suburban environment near Beijing: observed and modeled OH and HO₂ concentrations in summer 2006, *Atmos. Chem. Phys.*, 13, 1057-1080, 2013.

Mao, J. Q., Ren, X. R., Chen, S. A., Brune, W. H., Chen, Z., Martinez, M., Harder, H., Lefer, B., Rappenglück, B., Flynn, J., and Leuchner, M. (2010), Atmospheric oxidation capacity in the summer of Houston 2006: Comparison with summer measurements in other metropolitan studies, *Atmos. Environ.*, 44, 4107-4115, 10.1016/j.atmosenv.2009.01.013.

Martinez, M., Harder, H., Kovacs, T. A., Simpas, J. B., Bassis, J., Leshner, R., Brune, W. H., Frost, G. J., Williams, E. J., Stroud, C. A., Jobson, B. T., Roberts, J. M., Hall, S. R., Shetter, R. E., Wert, B., Fried, A., Alicke, B., Stutz, J., Young, V. L., White, A. B., and Zamora, R. J. (2003), OH and HO₂ concentrations, sources, and loss rates during the Southern Oxidants Study in Nashville, Tennessee, summer 1999, *J. Geophys. Res.*, 108, 10.1029/2003jd003551.

McKeen, S. A., Mount, G., Eisele, F., Williams, E., Harder, J., Goldan, P., Kuster, W., Liu, S. C., Baumann, K., Tanner, D., Fried, A., Sewell, S., Cantrell, C., Shetter, R. (1997), Photochemical modeling of hydroxyl and its relationship to other species during the Tropospheric OH Photochemistry Experiment, *Journal of Geophysical Research-Atmospheres*, 102, D5, 6467-6493.

Michoud, V., Kukui, A., Camredon, M., Colomb, A., Borbon, A., Miet, K., Aumont, B., Beekmann, M., Durand-Jolibois, R., Perrier, S., Zapf, P., Siour, G., Ait-Helal, W., Locoge, N., Sauvage, S., Afif, C., Gros, V., Furger, M., Ancellet, G., and Doussin, J. F. (2012), Radical budget analysis in a suburban European site during the MEGAPOLI summer field campaign, *Atmos. Chem. Phys.*, 12, 11951-11974, 10.5194/acp-12-11951-2012.

Mihelcic, D., Holland, F., Hofzumahaus, A., Hoppe, L., Konrad, S., Müsgen, S., Pätz, H.-W., Schäfer, H.-J., Schmitz, T., Volz-Thomas, A., Bächmann, K., Schlomski, S., Platt, U., Geyer, A., Alicke, B., and Moortgat, G., K. (2003), Peroxy radicals during BERLIOZ at Pabstthum: Measurements, radical budgets and ozone production, *Journal of Geophysical Research-Atmospheres*, 108, D4, 8254, doi:10.1029/2001JD001014.

Ren, X. R., Harder, H., Martinez, M., Leshner, R. L., Oligier, A., Shirley, T., Adams, J., Simpas, J. B., and Brune, W. H. (2003a), HO_x concentrations and OH reactivity observations in New York City during PMTACS-NY2001, *Atmos. Environ.*, 37, 3627-3637, 10.1016/s1352-2310(03)00460-6.

Ren, X. R., Harder, H., Martinez, M., Leshner, R. L., Oligier, A., Simpas, J. B., Brune, W. H., Schwab, J. J., Demerjian, K. L., He, Y., Zhou, X. L., and Gao, H. G. (2003b), OH and HO₂ chemistry in the urban atmosphere of New York City, *Atmos. Environ.*, 37, 3639-3651, 10.1016/s1352-2310(03)00459-x.

Ren, X., van Duin, D., Cazorla, M., Chen, S., Mao, J., Zhang, L., Brune, W. H., Flynn, J. H., Grossberg, N., Lefer, B., Rappenglück, B., Wong, K. W., Tsai, C., Stutz, J., Dibb, J. E., Jobson, B. T., Luke, W. T., and Kelley, P. (2013), Atmospheric oxidation chemistry and ozone production: Results from SHARP 2009 in Houston, Texas, *J. Geophys. Res.*, 118 5770-5780.

Rohrer, F., and Berresheim, H. (2006). Strong correlation between levels of tropospheric hydroxyl radicals and solar ultraviolet radiation. *Nature*, 442(7099), 184-187.

Sheehy, P. M., Volkamer, R., Molina, L. T., and Molina, M. J. (2010), Oxidative capacity of the Mexico City atmosphere – Part 2: A RO_x radical cycling perspective, *Atmos. Chem. Phys.*, 10,

6993-7008.

Shirley, T. R., Brune, W. H., Ren, X., Mao, J., Leshner, R., Cardenas, B., Volkamer, R., Molina, L. T., Molina, M. J., Lamb, B., Velasco, E., Jobson, T., and Alexander, M. (2006), Atmospheric oxidation in the Mexico City Metropolitan Area (MCMA) during April 2003, *Atmos. Chem. Phys.*, 6, 2753-2765.

Volkamer, R., Sheehy, P., Molina, L. T., and Molina, M. J. (2010), Oxidative capacity of the Mexico City atmosphere – Part 1: A radical source perspective, *Atmospheric Chemistry and Physics*, 10, 6969-6991.

Wong, K. W., Oh, H. J., Lefer, B. L., Rappenglueck, B., and Stutz, J. (2011), Vertical profiles of nitrous acid in the nocturnal urban atmosphere of Houston, TX, *Atmos. Chem. Phys.*, 11, 3595-3609, 10.5194/acp-11-3595-2011.

Wong, K. W., Tsai, C., Lefer, B., Haman, C., Grossberg, N., Brune, W. H., Ren, X., Luke, W., and Stutz, J. (2012), Daytime HONO vertical gradients during SHARP 2009 in Houston, TX, *Atmos. Chem. Phys.*, 12, 635-652, 10.5194/acp-12-635-2012.

Young, C. J., Washenfelder, R. A., Roberts, J. M., Mielke, L. H., Osthoff, H. D., Tsai, C., Pikelnaya, O., Stutz, J., Veres, P. R., Cochran, A. K., VandenBoer, T. C., Flynn, J., Grossberg, N., Haman, C. L., Lefer, B., Stark, H., Graus, M., de Gouw, J., Gilman, J. B., Kuster, W. C., and Brown, S. S. (2012), Vertically Resolved Measurements of Nighttime Radical Reservoirs; in Los Angeles and Their Contribution to the Urban Radical Budget, *Environ. Sci. Technol.*, 46, 10965-10973, 10.1021/es302206a.

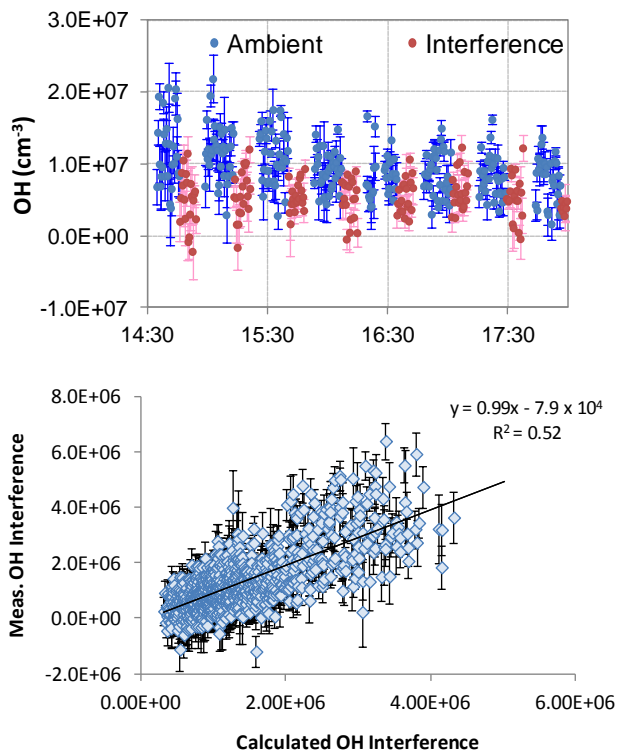


Figure S1: OH interference measurements from the CalNex-LA site. **Top:** Example time period during CalNex-LA of alternating 1-min average measurements of total OH signal (blue) and the interference signal measured after external addition of C_3F_6 (red). **Bottom:** 15 min average points of the calculated OH interference vs. the measured interference. The calculated interference is based on laboratory calibrations and found to be equivalent to $7500 (\pm 1000) \times [O_3] \text{ (ppbv)} \times [H_2O] \text{ (\%)} \times \text{LaserPower (mW)}$.

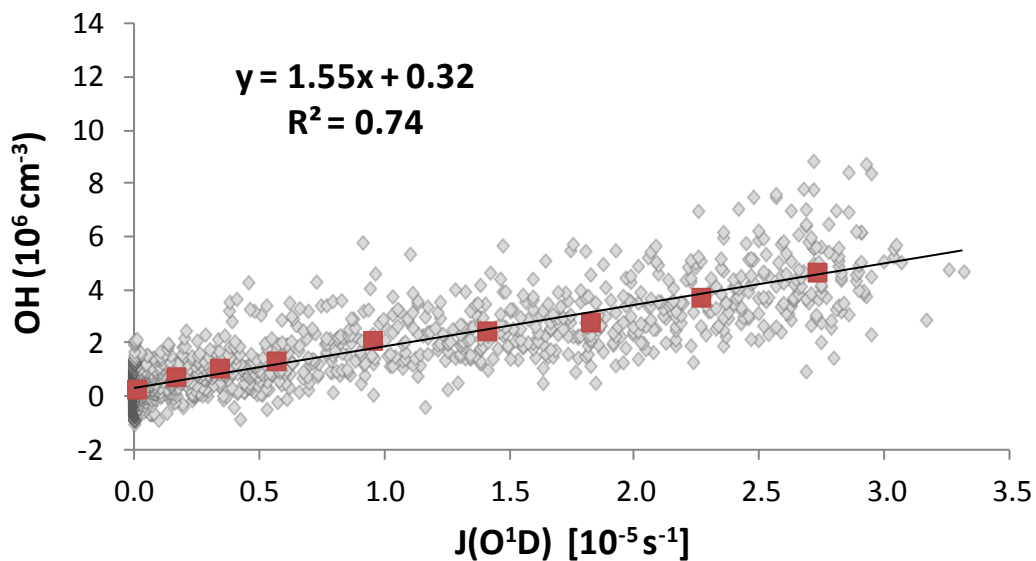


Figure S2: Correlation of $J(O^1D)$ photolysis rates and measured OH concentrations from the CalNex-LA site using a linear fit of all data points (gray). Average values are displayed in red.

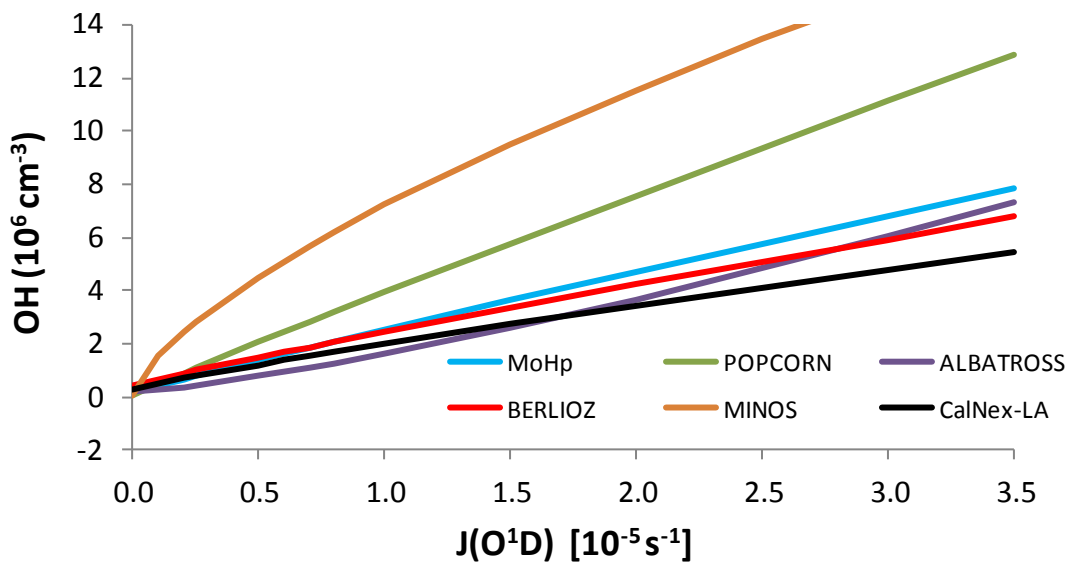


Figure S3: Power-law relationships (Eq.1) plotted from the Rohrer and Berresheim (2006) study along with the CalNex-LA results.

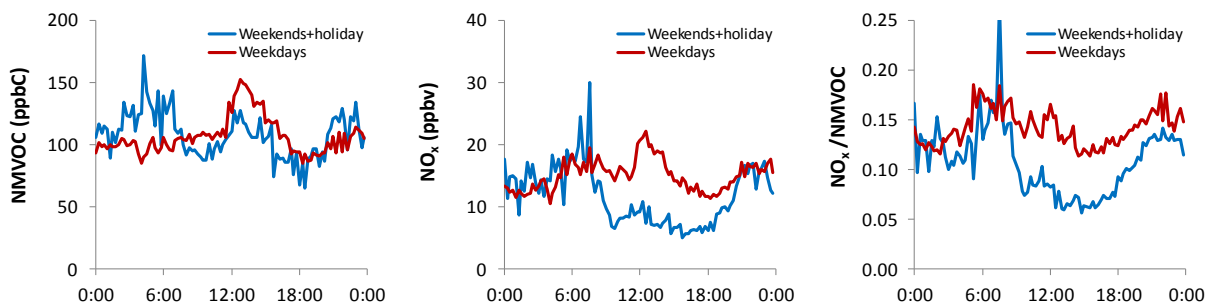


Figure S4: Weekend and weekday diurnal average plots of non-methane VOCs (NMVOCs), NO_x , and the ratio of NO_x/NMVOC observed at the CalNex-LA site.

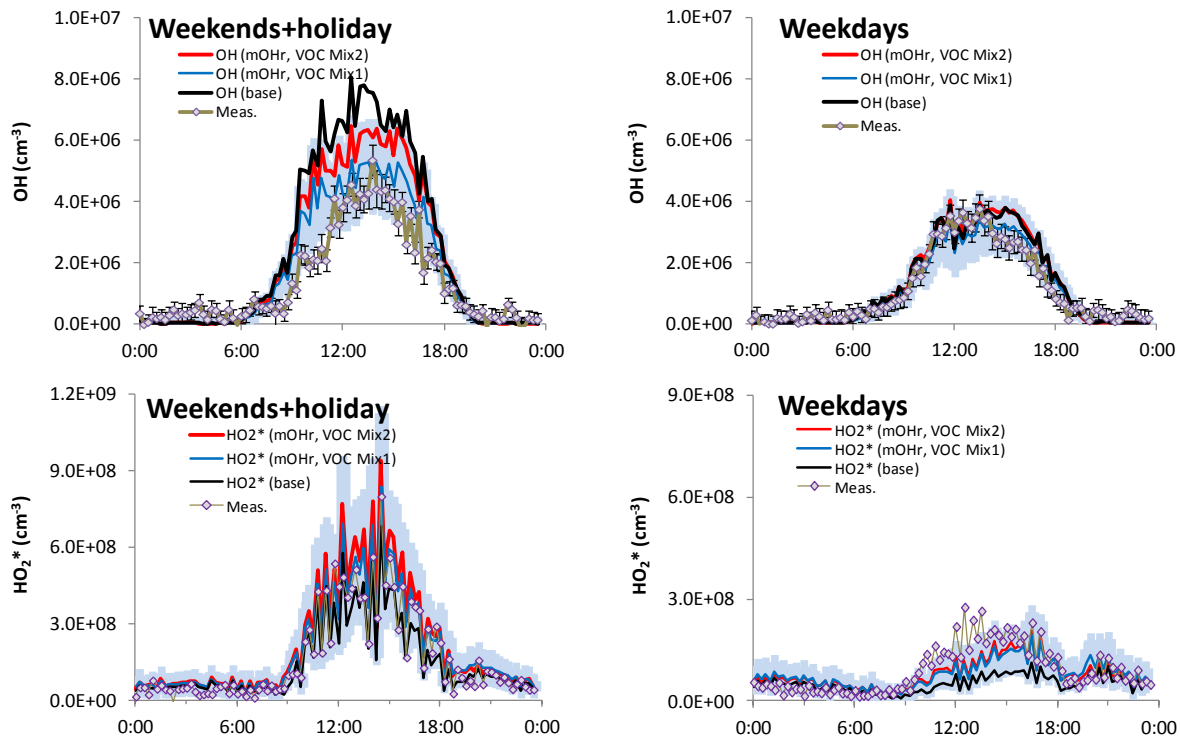


Figure S5: CalNex-LA diurnal average HO_x measurements and model results using two different VOC mixes for the increased reactivity scenario. The red trace incorporates alcohols and aldehydes to represent an OVOC mix, while the blue trace contains only saturated hydrocarbons and aldehydes. Modeled 1 σ uncertainties (shaded area) are 22.5% for OH and 35% for HO₂* and are only shown for the RACM2 results with the (mOHr, VOC Mix 1) scenario.

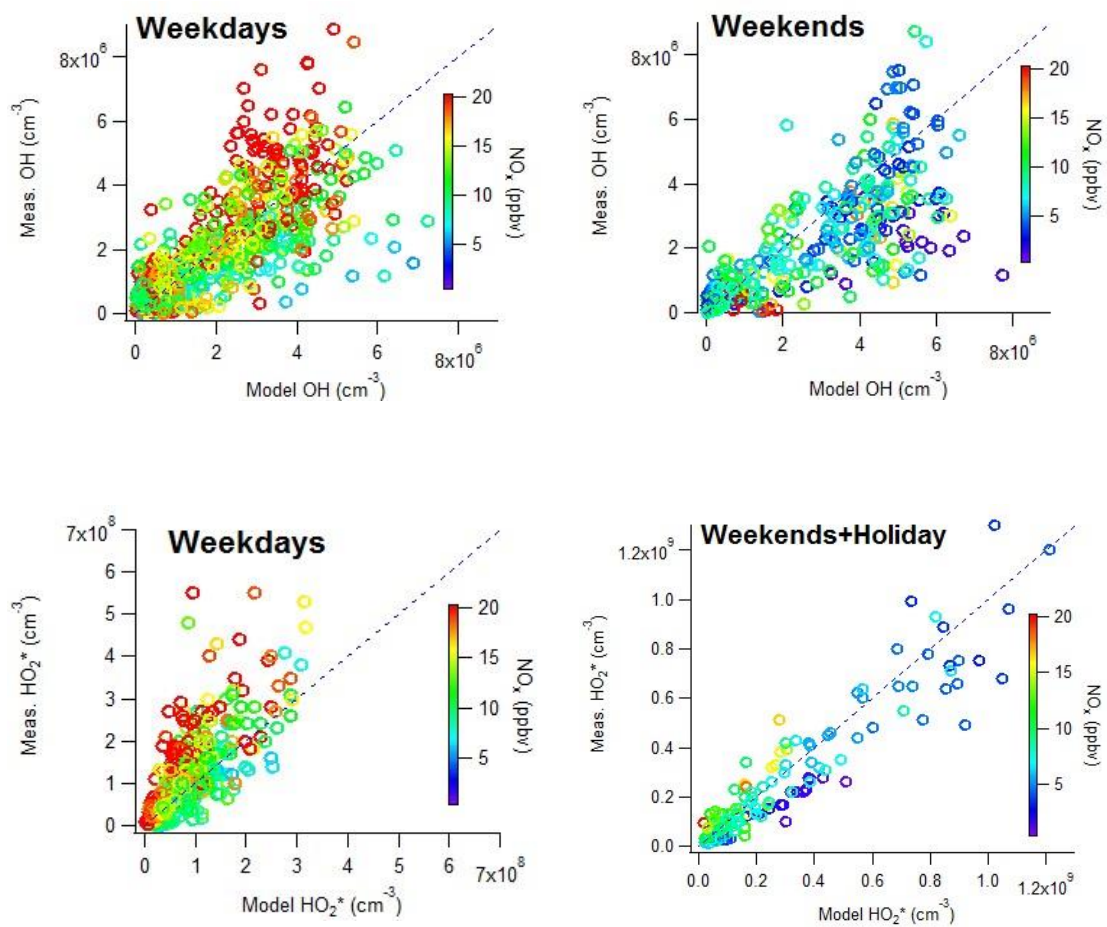


Figure S6: Correlation plots of the measured and modeled OH concentrations (top) and HO_2^* concentrations (bottom) as a function of NO_x .

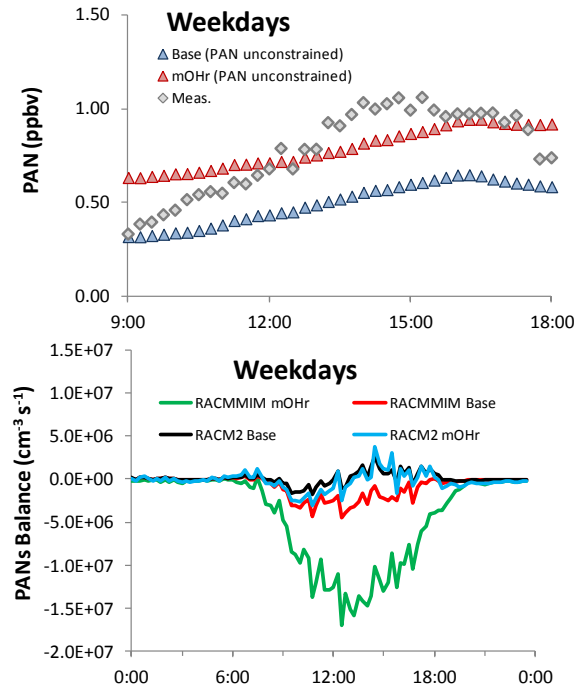


Figure S7: Measured vs. RACM2 model comparison of PAN in the base and mOhr scenarios (top). Comparison of equilibrium modeled PANs in the RACM-MIM and RACM2 models under base and mOhr scenarios (bottom).

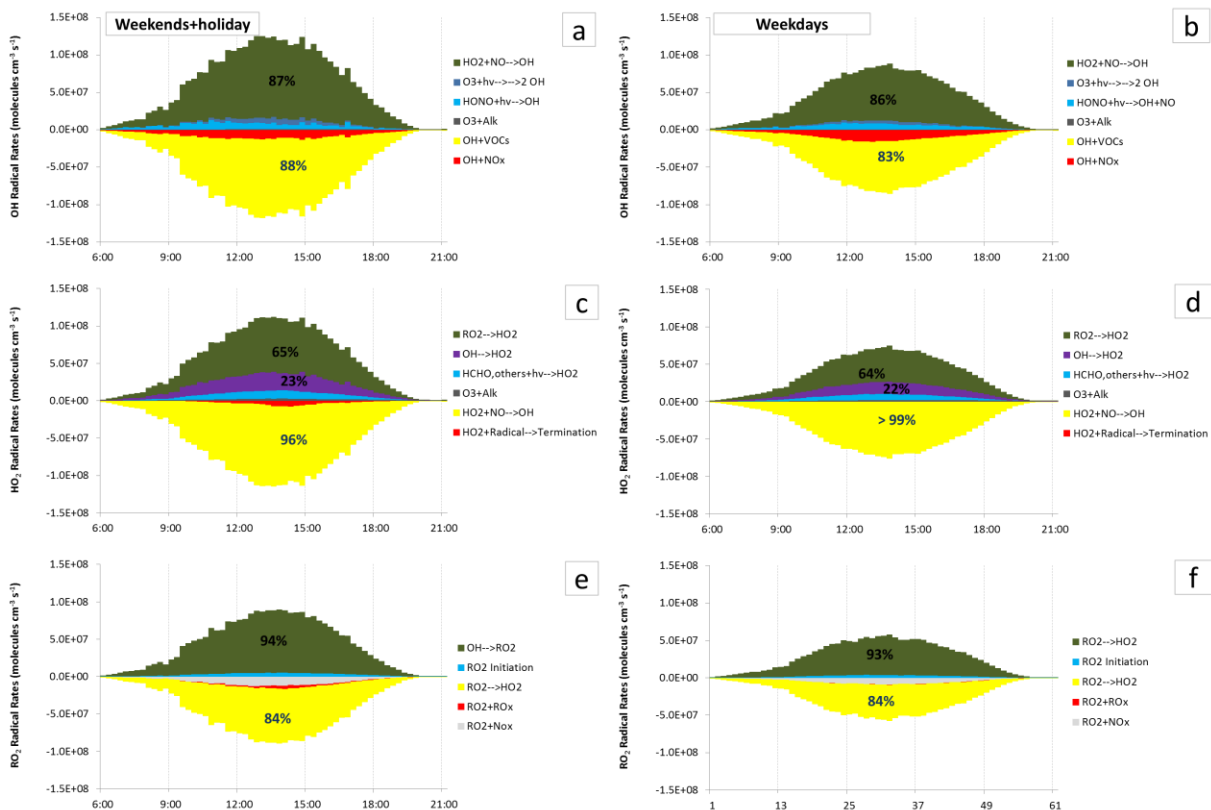


Figure S8: Diurnal average radical budgets from the ‘mOHr’ RACM2 model scenario for the weekends + holiday (left) and weekdays (right) with OH (top), HO₂ (middle) and RO₂ (bottom). Radical budgets balance initiation and termination routes with propagation routes (yellow, purple, and dark green). Percent contributions to either production or loss routes are given as 9a-6p averages.

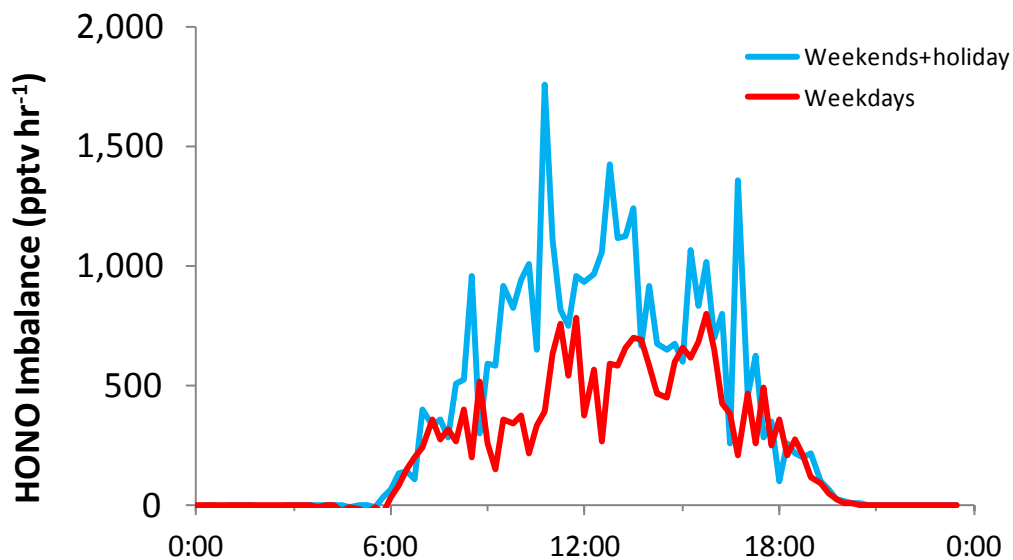


Figure S9: Diurnal average weekend + holiday average (blue) and weekday average (red) HONO imbalance (Photolysis of HONO – Gas-phase production of HONO) using measured OH, NO and NOAA IBCEAS HONO co-located from the top of the gas-phase tower at the CalNex-LA site.

Table S1: RO_x radical sources percent contribution comparison across urban campaigns

Campaign	Date ^a	Location	O ₃ Phot. (%)	HONO Phot. (%)	HCHO Phot. (%)	O ₃ +alk (%)	Other (%) ^b	Model	References
LAFRE	Sep. 1993 (1 d, 24 h) ^c	Los Angeles, CA, USA (LA basin)	31	11 ^{d,e,f}	21	6	32(86%)	CIT-AQ model + CACM ^g	Griffin (2004b)
		Azusa, CA, USA (LA basin)	28	6 ^{d,e,f}	17	5	44(64%)	CIT-AQ model + CACM ^g	Griffin (2004b)
		Riverside, CA, USA (LA basin)	32	4 ^{d,e,f}	14	3	47(54%)	CIT-AQ model + CACM ^g	Griffin (2004b)
	Sep. 1993 (1 d, 0800-2000) ^c	Claremont, CA, USA (LA basin)	25 ^h	27 ^{d,e,f,h}	27 ^h	12 ^{h,i}	9 (100%) ^{h,i}	PAMOL+CAL ⁱ	George et al., (1999)
LOOP/PIPAPO	May 1998 (2 d, 24 h)	Milan, Italy	23	26 ^k	39	10 ⁱ	2 (100%) ^{i,j}	--- ^m	Alicke et al., (2002)
BERLIOZ	Jul. 1998 (2 d, 24 h)	Pabstthum, Germany	38	17 ^k	37	7 ⁱ	1 (0%) ^{i,n}	--- ^m	Alicke et al., (2003) ^o
SOS	Jun.-Jul. 1999 (24 d, 24 h)	Nashville, TN, USA	54	9 ^{d,e,f}	29	8 ⁱ	--- ^p	McKeen et al., (1997) ^q	Martinez et al., (2003)
PUMA	Jun.-Jul. 1999 (14 d, 1100-1500)	Birmingham, UK	6	7 ^{d,e}	8	25	53 (97%)	0D+MCMv3.1	Emmerson et al., (2005, 2007)
PMTACS	Jun-Aug. 2001 (24 d, 24 h)	New York City, NY, USA	13	56 ^{f,r}	8	10 ⁱ	13(---) ^{i,s}	0D+RACM	Ren et al., (2003)
MCMA	Apr. 2003 (21 d, 24 h)	Mexico City, Mexico	19	11 ^{d,t}	19	14	37 (93%)	0D+MCMv3.1	Volkamer et al., (2010)
TORCH	Jul.-Aug. 2003 (34 d, 1100-1500)	Chelmsford, UK	14	10 ^{d,e}	8	20	50 (96%)	0D+MCMv3.1	Emmerson et al., (2007)
IMPACT	Jul.-Aug. 2004 (18 d, 0900-1500)	Tokyo, Japan	22	8 ^{d,e,f,h}	18	7 ^{h,i}	45 (66%) ^{h,i}	0D+RACM	Kanaya et al., (2007)
MILAGRO	Mar. 2006 (11 d, 0840-1840)	Mexico City, Mexico	6	35	24	19	16 (65%)	0D+RACM	Dusanter et al., (2009b)
PRIDE	Jul. 2006 (15 d, 1200-1600)	Pearl River Delta, China	32	12 ^t	37 ^u	10 ^v	9 (100%) ^w	0D+RACM-MIM-GK	Lu, et al., (2012)
TRAMP	Aug-Sep. 2006 (48 d, 0900-1800)	Houston, TX, USA	22-29	24-32	19-35 ^x	2-10 ⁱ	5-18 (---) ^{i,x}	0D+5 mechanisms ^y	Chen et al., (2010)
CARE	Aug-Sep. 2006 (8 d, daytime)	Beijing, China	15 ^z	24 ^{t,z}	27 ^z	< 18 ^{z,aa}	> 16 (---) ^{z,aa}	0D+RACM-MIM-GK	Lu, et al., (2013)
SHARP	Apr-May 2009 (47 d, 24 h)	Houston, TX, USA	30	22	14	13 ⁱ	21 (71%) ⁱ	0D+5 mechanisms ^y	Ren et al., (2013)
MEGAPOLI	July 2009 (1d ^{ab} , 0700-1900)	Paris, France	23	35	15	8	19 (92%)	0D+MCMv3.1	Michoud et al., (2012)
CalNex	May-Jun 2010 (25 d, 0900-1800)	Pasadena, CA, USA (LA Basin)	12	28	9	14	37 (86%)	0D+RACM2	This study

^aNumber of days and averaging time (italicized) for the radical budget given in parentheses; ^bC2 and higher carbonyl photolysis portion of 'other' given in parentheses; ^cThe LAFRE campaign was carried out in Sep. 1993, but the two modeling analyses presented here focused on different days in the campaign; ^dHONO mixing ratios were not constrained in the model; ^eMechanism includes a heterogeneous HONO source via 2NO₂+H₂O→HONO+HNO₃; ^fHONO photolysis contributions are net (HONO photolysis – gas-phase HONO production) values; ^gCalifornia Institute of Technology 3D Air Quality emissions based model coupled with the California Atmospheric Chemistry Mechanism (Griffin et al., 2002, 2004a); ^hEstimated values from reference publication; ⁱDoes not account for new RO₂ formation, thus is a lower limit for this category; ^jNumerical integrator based on Gear (1971) coupled with mechanism detailed in Lurmann et al., (1987); ^kGross OH production from HONO photolysis based on measurements of HONO in the early morning, while daytime HONO concentrations are estimated based on a steady-state expression including 2NO₂+H₂O→HONO+HNO₃, direct emission of HONO (only for LOOP/PIPAPO), and HONO loss by photolysis; ^lTypical values of OVOCs used from Alicke et al., (2002) to calculate OVOC+hv; ^mCalculations only based on measured concentrations; ⁿLimited by measurement availability, higher carbonyl photolysis is not included; ^oModeling of radical budgets is performed by Mihelcic et al., (2003) but percent contribution values are not given nor are they estimated here; ^pNot provided in the publication, but was indicated that primary HO_x initiation routes are those provided; ^qPhotochemical steady-state model using an updated version of recently used mechanism (McKeen et al., 1997); ^rMao et al., (2010) and Ren et al., (2013) have indicated that the OH concentrations in this study should be increased by a factor of ~1.4, therefore the net HONO values here should be considered an upper limit; ^sBreakdown of the 'other' category not provided in publication; ^tMechanism includes homogenous NO₂+H₂O→HONO+OH reaction; ^uHCHO not constrained to measurements in the model; ^vTypical O₃+alkene provided here for comparison to other campaigns; ^wAdditional routes in the 'other' category besides carbonyl photolysis not provided in the reference publication; ^xChen et al., (2010) groups HCHO with other carbonyls in the OVOC+hv and states the majority is from HCHO photolysis. Thus total OVOC+hv is given in the HCHO+hv column and other routes besides carbonyl photolysis are given in the 'other' column; ^yValues given are the range of outputs from the 5 mechanisms compared in the HO_x budget; ^zValues are for the southerly wind direction during the campaign; ^{aa}Lu et al., (2013) states that 16% of RO_x radical initiation is from higher carbonyl photolysis but doesn't provide the breakdown for the rest of the routes (i.e. O₃+alkenes and others); ^{ab}MEGAPOLI spanned 31 days but the radical budget was performed on campaign average values